CHAPTER IX.C

IRON FISCHER-TROPSCH CATALYSIS - PROPERTIES OF AN ULTRAFINE IRON OXIDE CATALYST

ABSTRACT

Slurry phase Fischer-Tropsch synthesis has been conducted starting with an ultrafine iron oxide catalyst with an average particle size of 30Å. Catalyst activity gradually increased during the first 400 hour of synthesis and then remained stable for 250 days. Potassium promotion greatly increased the initial activity of the catalyst; however, the stability decreased. The CO conversion of the unpromoted catalyst was found to vary linearly with the reciprocal of the space velocity up to 60% conversion. Alkene selectivity increased with increasing space velocity but remained constant above GHSV = 2.0. Secondary reactions are believed to account for the higher alkane content at low space velocity. Methane, ethane and alkane formation increased with increasing hydrogen partial pressure up to a H_2/CO ratio of 1. CO conversion is highest at lowest CO partial pressure and likewise for hydrogen. In general it is observed that this ultrafine catalyst is not as active as precipitated catalysts and has poor selectivity for alkene synthesis.

INTRODUCTION

The Fischer-Tropsch Synthesis (FTS) has received much attention since its discovery (IX.C-1, IX.C-4, IX.C-5 IX.C-15, IX.C-17, IX.C-23). However, the complexity of the products and the range of conditions where the reaction has been carried out make it difficult to make direct quantitative comparisons of the studies. While a range of metals can be utilized for the catalyst preparation for syngas

conversions, the FTS is usually restricted to catalyst formulations based on iron or cobalt. Even when one focuses on the iron catalysts, the catalyst formulations vary over a wide range, both in physical properties and chemical composition.

The FTS is accompanied by a large heat evolution that occasionally results in superheating of the catalyst surface, usually resulting in loss of activity. One of the detriments to the commercialization of the FTS has been the engineering designs that result in expensive reactors to handle the heat of reaction. To allow for more efficient heat transfer, liquid [slurry] phase synthesis has been introduced (IX.C-21). For the most part, the early work involved the use of pulverized catalysts prepared by precipitation or by a fused iron procedure. However, recent work has been carried out utilizing spherical particles prepared by spray drying (IX.C-2, IX.C-3).

In the slurry phase synthesis, heavy wax accumulates in the reactor so that it is necessary to continuously, or periodically, withdraw samples from the reactor. Since the withdrawn sample contains catalyst, it is essential that the catalyst be recovered for return to the reactor. For separations based upon settling or filtration, it is desirable that reasonably large (~25-100 micron) sized catalyst particles be utilized.

The impact of diffusion of the reactants and products upon catalyst activity and product selectivities becomes an important consideration for slurry phase synthesis with larger catalyst particles. For this reason, it is of interest to obtain FTS data for slurry phase synthesis with a catalyst of small particle size even though this catalyst could not be easily utilized in a commercial operation.

Ultrafine particles are nominally considered to be less than 0.1 μm. The commercial availability of an iron oxide with a narrow particle size range and an

average diameter of about 3 nm offers an opportunity for the study of ultrafine iron based catalysts in the FTS.

Itoh and coworkers (IX.C-8 - IX.C-14, IX.C-18, IX.C-19) have utilized ultrafine catalysts in FTS. These catalysts ranged from slightly larger than 20 nm to about 80 nm and were prepared by several techniques including: (1) hydrogen reduction of the chlorides in the vapor phase at 1,000°C, (2) reduction of an aqueous solution of metal chloride with KBH_4, and (3) a gas evaporation method to produce α-Fe (IX.C-16, IX.C-20). In general, it was observed that the ultrafine catalyst had a higher activity than a precipitated catalyst with a similar composition when compared under similar reaction conditions. The catalyst containing mainly iron showed high catalytic activity and oxygenates. Ultrasonic irradiation of a suspension increased catalyst dispersion, and the activity (IX.C-8). The authors found chain growth occurred on dual sites, with one assigned to a potassium-promoted site. Thus, these authors appeared to agree with Schliebs and Gaube (IX.C-22) in assigning the alkali metal responsibility for a two-alpha Anderson-Schulz-Flory (ASF) chain growth to describe the products. However, in a later paper these authors show that a two-alpha plot was needed to describe the products produced by either an unpromoted or an alkali promoted catalyst (IX.C-10). Itoh et al. (IX.C-12) found that preoxidation of the α-Fe ultrafine catalyst enhanced the catalytic activity and speculated that this was due to the slower sintering of the catalyst.

A commercial iron oxide with a particle size of 3 nm is now available; this is much smaller than the 20-80 nm ultrafine particles utilized by Itoh and coworkers (IX.C-8 - IX.C-14, IX.C-18, IX.C-19). We have found that even though the oxide can

be converted to the carbide by CO pretreatment, the catalyst under synthesis conditions is reoxidized so that a dominant fraction of the working catalyst is present as an oxide form after about 100 hours exposure to synthesis gas (IX.C-6, IX.C-7). The FTS requires considerable time on stream before steady state conditions are attained. Since the activity-selectivity data of Itoh et al. were for only the initial 6-hour reaction period it is desirable to obtain FTS data for the smaller ultrafine iron oxide catalysts at larger times on stream. Data for operation up to six months on-stream are reported herein.

EXPERIMENTAL

Catalyst

A commercial sample (Mach, Inc.) of ultrafine iron oxide was utilized for these experiments. The material, as received, does not contain significant water; however, the material is very hygroscopic and will quickly adsorb up to 15 wt.% moisture upon a brief exposure to the atmosphere. If proper precautions - slow heating with evacuation - are taken, the measured surface area of 270-310 m^2/g agrees with the one reported by the vendor. The particle size we measured by TEM is in the range of 1-3 nm; this size agrees very well with the surface area value reported by the vendor. The vendor reports that the material is α-Fe_2O_3. The TEM diffraction pattern of the as-received material exhibits two diffuse rings which do not have the appropriate relative intensities expected for α-Fe_2O_3. The high resolution transmission electron microscopy (HRTEM) data suggest that the material is γ-Fe_2O_3.

Procedure

The as-received iron oxide (95 g) was added to melted octacosane ($C_{28}H_{58}$) to produce a slurry that contained 20 wt.% iron oxide in a 1-liter autoclave that was fitted

with a magnetically driven stirrer, a tube fitted with a stainless steel fritted filter that extended below the liquid level for withdrawing wax from the reactor and a vapor exit line.

Catalyst Pretreatment.

The reactor, after pressure testing, was heated to 260°C at a rate of 1.5 - 2.0°C/min. During heat-up CO at 100 psig was passed through the stirred (750 rpm) reactor at a rate of 0.14 NL/hr/g Fe. After attaining a pretreatment temperature of 260°C, the pretreatment of the sample was continued for 24 hours in CO. The sample was maintained at this temperature for 24 hours before switching to a synthesis gas feed ($H_2/CO = 1$).

Reaction Run

The run was conducted in a continuous stirred tank reactor (CSTR). The hydrogen and CO flow rates were controlled by a thermal mass flow regulator (Brooks Instrument); after flow regulation the two gases were mixed in a 0.5 ℓ pressure vessel prior to entering the reactor. The reaction was conducted at 260°C and 100 psig (8 atm. absolute) with the stirring at 750 rpm. At 1248 hr. the synthesis was stopped to change the gas flow control valve. During the first 3111 hrs (130 days) of operation the feed gas had a composition of $H_2/CO = 1.0$ but the flow rate was varied as outlined in Table I. Following this period, studies were made with a total gas flow of 2.50 NL/hr/g Fe but with the various H_2/CO ratios shown in Table III.

Table I

The Flow Rate of the H_2/CO = 1.0 Gas Mixture During 0-3111 Hours of Operation

Time Period, Hr.	Gas Flow, NL/hr/g Fe
0-672	0.27
672-1584	1.18
1584-1942	3.20
1942-2180	2.00
2180-2348	4.20
2348-3111	2.50

The CSTR was operated so that a gas/liquid stream exited the reactor through a tube fitted with a metal porous filter (0.5 μm). The effluent for the first 3234 hours passed sequentially through three traps maintained at 60, 50 and 3°C respectively; after 3234 hours the trap temperatures were 160°C, 60°C and 3°C, respectively.

The gas exiting the 3°C trap passed through a Tescom pressure regulator to reduce the exit product stream pressure to atmospheric pressure. The depressurized gas stream was sampled by on-line injection to either a Carle Gas Analyzer or to a GC fitted with a Porpack Q column for hydrocarbon analysis.

The Carle gas analyzer was utilized for quantitative determinations of CO, H_2, CO_2, CH_4, C_2H_4, C_2H_6, C_3H_6, C_3H_8 and the butane/butene compounds. The instrument was calibrated using a standard mixture of the gases to be analyzed (supplied by Matheson Gas Products, Inc.) to obtain factors to enable the moles of each of the above compounds in the exit gas stream to be calculated.

The higher hydrocarbons (C_4 - C_{11}) in the exit gas were determined using a GC fitted with a Porpack Q column operated at 100°C for 1 min., then programmed at 8°C/min. to 245°C. The alkene/alkane fractions were not separated using this column;

thus, this column provided data for the carbon number fractions for calculation of the mole fraction of each carbon number grouping.

The three traps were sampled at intervals (usually every 24 hours) and the mass of each sample was obtained. The 3°C trap sample contained both an oil and aqueous phase; the two phases were separated and the mass of each phase was determined.

The aqueous phase was analyzed for water and oxygenates using a GC fitted with a Porpack Q column operated at 100°C for 1 min., then programmed at 8°C/min. to 245°C.

The oil phases in the 60°C and the 3°C sample traps were combined according to the mass balance for these fractions. A weighed fraction of ortho-xylene was added as an internal standard. For the temperature program with the DB-5 column, hydrocarbons above about 35 carbon numbers did not quantitatively elute from the column. The use of three traps at 120°C, 60°C, and 3°C decreased the amount of higher hydrocarbons in the combined sample (omitting the $120°C^+$ wax) to be analyzed and the internal standard provide a means of accounting for any fraction of the sample that did not elute.

RESULTS

The flow of the synthesis gas ($H_2/CO = 1$) was varied during the initial period of the conversions. Due to analytical difficulties only gas analyses are available during the first periods of operation (up to about 3300 hours on stream). The variation in conversion for variations in the flow rates are given in (Figure IX.C-1). The conversion of CO varies linearly with the reciprocal of the space velocity (time) up to about 60% CO conversion; above this conversion level the rate of conversion of CO dramatically

decreases. At the same time, the conversion of hydrogen depends upon the extent of CO conversion. At low CO conversions, the hydrogen conversion exceeds that of the CO; however, with increasing CO conversions the conversion of hydrogen relative to CO decreases and finally, at higher conversions, the CO conversion exceeds that of the hydrogen (Figure IX.C-2). This is obviously a result of the role of the water-gas-shift reaction.

During the initial synthesis period at a low CO/H_2 flow rate there is a gradual increase in conversion during about 400 hours into the syngas conversion period (Figure IX.C-3). During the other periods the conversion levels are reasonably stable (Figures IX.C-4 and IX.C-5 are representative). The initial conversion levels parallel changes in the catalyst composition following exposure to synthesis gas and will be covered in the Discussion Section. During the first 3111 hours (130 days) of operation the catalytic activity did not appear to decline; during each of the periods of operation in Table I , except for the first 400 hours of operation, the activity remained essentially constant.

The percentage of alkane in the C_2 - C_4 products did not depend on the flow rate above about 2.0 NL/gFe-hr for H_2/CO = 1 at 7 atm. psig and 260°C (Table II); below this flow the alkane fraction increases due to secondary reactions. The C_2 fraction contains 90% or more of the alkane; the olefin content increases with increasing carbon number.

Table II

The Alkane Percentage for the C_2, C_3 and C_4 Hydrocarbons During Syngas Conversion at Various GHSVs (T=260, 7 atm psig, and H_2/CO = 1.0)

GHSV, NL/g Fe/hr	C_2^a	C_3^a	C_4^a
1.18	.96	0.73	0.51
2.0	0.95	0.57	0.39
2.5	0.90	0.54	0.39
3.2	0.90	0.54	0.38
4.2	0.89	0.51	0.37

a Defined as $C_i/C_i + C_i^=$ where i is the carbon number, C_i and $C_i^=$ are the alkane and alkene, respectively, with carbon number i.

A series of runs were made in which the total gas flow rate remained constant at 2.5 NL/g Fe/hr but the feed gases contained helium so that the H_2/CO ratio could be varied from 0.5 to 2.0 (Table III). During each interval of constant H_2/CO feed, the conversion remained very constant. The data in Figures IX.C-5 and IX.C-6 represent the CO, H_2 and total feed conversion with time data at the high (2.0) and low (0.5) H_2/CO ratios, respectively. As expected, the H_2 conversion exceeds that of CO at the low H_2/CO ratio and the CO conversion exceeds that of hydrogen at the high H_2/CO ratio.

Table III

The Variation of H_2/CO Ratio at a Total Gas Flow of 2.5 NL/hr/g Fe During the Hours of Operation Indicated

Time Period, Hr.	H_2, %	CO, %	He, %	H_2/CO
3111 - 3426	50	33.3	16.6	1.5
3426 - 3788	50	25	25	2.0
3788 - 4052	25	50	25	0.5
4052 - 6144	37.5	50	12.5	0.75

The water-gas-shift (WGS) reaction is considered to be an important component of the Fischer-Tropsch synthesis with an iron catalyst. However, for this

unpromoted ultrafine catalyst, the WGS activity is low. The equilibrium constant for the reaction:

$$CO_{(g)} + H_2O_{(g)} \rightleftharpoons CO_{2_{(g)}} + H_{2_{(g)}}$$

at 260°C is about 62. Thus, the data in Figure IX.C-7 indicate that the WGS reaction never attains more than 5% of the equilibrium value. The data for $H_2/CO = 1$ were obtained without helium dilution (data point ▲ in Figure IX.C-7) and appear to fit reasonably well a curve defined by the data generated at lower partial pressures of H_2 or CO.

The production of CH_4 and C_2H_6, as a percentage of the total C_1^+ products (excluding CO_2), depends strongly on the H_2/CO ratio. For the lower H_2/CO ratios the amount of $CH_4 + C_2H_6$ is low, then rapidly increases as the H_2/CO ratio approaches 1, and with further increase in the H_2/CO ratio the increase becomes more gradual (Figure IX.C-8).

The percent of alkane for the C_2 - C_4 carbon number fractions shows a dependence on the H_2/CO ratio (Figure IX.C-9). However, at or above a H_2/CO ratio of 1.0, there is little, if any, change in the extent of hydrogenation.

The extent of hydrogenation for this unpromoted ultrafine iron oxide catalyst is higher than for a promoted iron catalyst under similar conditions (IX.C-24).

In the following, the conversions of CO and H_2 are compared as the H_2/CO ratio (and consequently the partial pressure of one of the reactants) is varied. The percentage of conversion of CO is highest at the lowest CO partial pressure, and a similar observation applies for hydrogen (Figures IX.C-10 and IX.C-11).

The percentage conversion of CO, H_2 and (CO + H_2) is lowest at intermediate values of H_2/CO; however, the minimum percentage conversion for each of the components occurs at a different H_2/CO ratio (Figure IX.C-12). Unfortunately, the data in Table II do not permit a comparison of either H_2 or CO conversions where the one variable is held at a constant partial pressure and the other varied over 3 or more partial pressures.

A typical plot showing the variation of the alkane fraction, defined as (n-alkane)$_i$/(n-alkane + 1-alkene + (trans- + cis-)-2-alkene)$_i$, with carbon number is shown in Figure IX.C-13. A similar shaped plot was obtained under similar conditions with a doubly promoted fused iron (UCI C-73) catalyst with the following exception that for the promoted catalyst (IX.C-24) : (1) the products were more olefinic throughout the carbon numbers, (2) the minimum at $C_4^=$ was lower (0.2) and was much broader, (3) the fraction of alkanes increased more slowly in the C_5 - C_{20} range, and (4) the products at C_{20} and higher were still only about 0.8 alkanes. Thus, the unpromoted ultrafine iron catalyst is a better alkene hydrogenation catalyst than the C-73 promoted catalyst; however, it cannot be defined from the data whether the higher alkane production is due to the formation of alkanes as primary products or by secondary hydrogenation reactions. Changing the H_2/CO ratio does not appreciably change the alkane selectivity with carbon number (Figure IX.C-14). However, even with a 20% catalyst slurry, it takes 10 or more days to turn over the reactor wax volume so that a steady-state wax composition was not obtained for most of the data shown in Figure IX.C-14.

The data for the Anderson-Schulz-Flory (ASF) plot in Figure IX.C-15 give two ASF slopes; these data are representative of the last half of the run period. The line used for on-line sampling of hydrocarbons for analysis by the Porpack Q column is heat traced; however, there is accumulation of C_9^+ hydrocarbons due to condensation so that the inclusion, or the exclusion, of the C_9^+ alkanes determined using the Porpack Q column will cause the C_9 - C_{11} products to either fall above, or below, respectively, the trend shown in Figure IX.C-15.

Data typical of the fraction of 1-alkene present in the 1- plus (cis plus trans)-2-alkene for each carbon number fraction from C_4 through C_{25} are shown in Figure IX.C-16. With most promoted iron catalysts the primary product is the 1-alkene; however, with this unpromoted ultrafine iron catalyst the dominant alkene product is not the 1-alkene. Presumably this is due to the more rapid hydrogenation of the 1-alkene than the interval alkenes. For the carbon number fractions above about 20 the alkenes are present in such small amounts that an accurate measure of this ratio is not possible.

A shorter run of about 2000 hours (~84 days) was made with an ultrafine catalyst which contained 0.5 wt.% potassium. In this run sufficient potassium t-butoxide was added to a slurry in the CSTR that contained 10% iron oxide to provide a catalyst with 0.5 wt.% K. The slurry oil used for start-up was an ethyl C_{30} oil. The pretreatment was in CO and was the same as used for the unpromoted catalyst. During the first 1368 hours of the run the gas velocity was 3.2 NL/hr/g Fe; at 1368 hours the flow was decreased to 2.0 NL/hr/g Fe. The run was conducted at 260°C, 100 psig and $H_2/CO = 1$.

The conversion with this catalyst was initially high but the catalyst showed a gradual decline in activity during the run for the GHSV = 3.2 (Figure IX.C-17). Decreasing the space velocity produced an increase in conversion which was then followed by a decline in activity.

The WGS activity for this catalyst was greater than was observed with the unpromoted iron catalyst. However, $K_{apparent}$ appeared to gradually decline from 10 to 5 during the course of the run. Even at the end of the reaction period, $K_{apparent}$ was larger than was ever observed for the unpromoted iron catalyst (Figure IX.C-6).

The alkali, as expected, caused the catalyst to produce a larger fraction of alkenes in the C_2 - C_4 products (Figure IX.C-18). Likewise, the alkane fraction of the carbon number products were shifted to more olefinic product (Figure IX.C-19 versus Figure IX.C-12).

The ASF plot for the alkali containing catalyst (Figure IX.C-20) produced a curve that resembled the pure iron catalyst. The alpha value defined by the C_1 - C_{10} products was 0.62 for the alkali containing catalyst versus 0.65 for the unpromoted iron oxide. Likewise, the second alpha values, defined by the C_{10}-C_{30} products were 0.77 for the unpromoted catalyst and 0.82 for the promoted catalyst.

DISCUSSION

The activity of the unpromoted catalyst based on ultrafine iron oxide was surprisingly resistant to aging; the catalytic activity was essentially constant for nearly 250 days. In comparison, the same ultrafine iron oxide that contained 0.5% K showed a high initial activity but the activity gradually declined. Even so, the potassium

promoted catalyst was operated for about 1350 hours (~56 days) while the activity, based on CO conversion, declined from about 82% to 30% (an average of 0.92%/day). In spite of the decline in activity the potassium promoted catalyst had an activity after 56 days (CO conversion of 30% at 3.2 NL/gFe•hr) that was about the same as the unpromoted iron catalyst for a comparable flow rate. However, the two catalysts were not run under the same conditions; the unpromoted catalyst was utilized as a 20 wt.% while the promoted catalyst run utilized only 10 wt.% slurry.

Itoh et al. (IX.C-8 - IX.C-14, IX.C-18, IX.C-19) found that their ultrafine catalyst was more active than a precipitated iron catalyst. We did not find this to be the case since several of our precipitated catalysts have a higher activity than the ultrafine catalyst. However, our precipitated catalyst can also be considered to be an ultrafine catalysts if the definition is based upon the size of the ultimate particles rather than the size of an agglomeration of particles. Our precipitated catalysts, starting with FeOOH and Fe_2O_3, produce conversions as high as 80-90% under conditions where the ultrafine catalyst used in this study produced only about 30% conversion. Thus, our data indicate that precipitated catalysts may be more active than ultrafine catalysts prepared by other methods.

The conditions utilized by Itoh et al. were so different from those of the present studies that a direct comparison cannot be made. Their CO conversion at 220°C and 442 psig were slightly higher than our conversion at 270°C and 100 psig.

Both the unpromoted and potassium promoted ultrafine oxide produced products which fit a two-alpha ASF plot. However, the addition of potassium only slightly decreased the first alpha value (from 0.65 to 0.62) and slightly increased the higher alpha value (from 0.77 to 0.82). The presence of potassium had an influence

upon the selectivity for alkene and produced a higher fraction of alkene for the C_2 - C_{20} products. However, the impact of potassium promotion was less than normally expected for promotion by alkali.

Characterization studies (IX.C-6, IX.C-7) indicate that pretreatment of the ultrafine iron oxide with CO for 24 hours converts most, or all, of the oxide to a mixture of iron carbides. Thus, in the present activity studies it appears that the catalyst initially is predominantly in the carbide form, and exhibits low catalytic activity. During the syngas conversion, a major fraction of the iron carbides initially present are converted to Fe_3O_4; the rate and extent of carbide conversion to oxide depends upon the syngas conversion and the reaction time. However, during 100-300 hours of syngas conversion at 60 to 70%, or even higher, conversion of the carbide to oxide occurs. To the extent that the catalyst used in the current study parallels the earlier characterization studies, the iron oxide produced from the iron carbide is more active than the iron carbide. An increase in activity was anticipated from the conversions, based on only gas analysis, measured in the pretreatment studies. The magnitude of the activity increase observed in this study was, however, not anticipated.

In summary, an ultrafine iron oxide has exhibited remarkable maintenance of catalytic activity for a 150 day operating period. The addition of potassium at a level of 0.5% increased the activity over that of an unpromoted iron oxide. After 56 days of continuous operation the activity of the potassium promoted catalyst had declined to become equivalent to that of the unpromoted catalyst; however, while the unpromoted ultrafine iron oxide catalyst retained a constant activity the potassium promoted catalyst continued to decline in activity. Neither the unpromoted nor potassium promoted catalyst exhibited good selectivity for alkenes.

ACKNOWLEDGMENT

This work was supported by DOE contract #DE-AC22-90PC90049 and the Commonwealth of Kentucky.

REFERENCES

IX.C-1. Anderson, R. B., 1984. "The Fischer-Tropsch Synthesis", Academic Press, New York.

IX.C-2. Bhatt, B. L.,.1992. "Liquid Phase Fischer-Tropsch Synthesis in a Bubble Column", Liquefaction Contractor's Review Conference, Pittsburgh, Pa, September 22-24.

IX.C-3. Davis, B. H., and F. L. Tungate in 1991. "Liquefaction Contractor's Review Meeting Proceedings", (G. J. Steigel and R. D. Srivastava, eds.), Pittsburgh, PA, September 3-5.

IX.C-4. Fischer, F., and H. Tropsch, 1923, 1924. *Brennst. Chem.*, **4**, 276; **5**, 217.

IX.C-5. Henrici-Olivé, G., 1984. "The Chemistry of the Catalyzed Hydrogenation of Carbon Monoxide", Spring-Verlag, Berlin.

IX.C-6. Huang, C. S., L. G. Xu and B. H. Davis, 1993a. *Fuel Sci. Technol. Int.*, **11**, 639.

IX.C-7. Huang, C. S., B. Ganguly, G. P. Hufman, F. E. Huggins and B. H. Davis, 1993b. *Fuel Sci. Technol. Int.*, **11**, 1289.

IX.C-8. Itoh, H., E. Kukuchi and Y. Morita, 1987. *J. Japan Petrol. Inst.*, **30**, 324.

IX.C-9. Itoh, H., H. Tanabe and E. Kikuchi, 1989. *Appl. Catal.*, **47**, L1.

IX.C-10. Itoh, H., H. Hosaka, T. Ono and E. Kikuchi, 1988. *Appl. Catal.*, **40**, 53.

IX.C-11. Itoh, H., and E. Kikuchi, 1990. *Appl. Catal.*, **67**, 1.

IX.C-12. Itoh, H., S. Nagano and E. Kikuchi, 1991a. *Appl. Catal.*, **67**, 215.

IX.C-13. Itoh, H., S. Nagano, T. Urata and E. Kikuchi, 1991b. *Appl. Catal.*, **77**, 37.

IX.C-14. Itoh, H., T. Ono and E. Kikuchi, 1990. *Bull. Sci. & Eng. Res. Lab., Waseda, Univ.*, No. 129, pp 90-93.

IX.C-15. Kaliaguine, S. (Ed.), 1988. "Keynotes in Energy Related Catalysis", Elsevier, Amsterdam.

IX.C-16. Kashu, S., M. Nagase, C. Hayashi, R. Uyeda, N. Wada and A. Tasaki, 1974. *Japan J. Appl. Phys.*, Suppl. 2, Pt. 1, 491.

IX.C-17. Keim, W. (Ed.), 1983. "Catalysis in C_1 Chemistry", D. Reidel Pub. Co., Boston.

IX.C-18. Kikuchi, E. and H. Itoh in 1988, "Methane Conversion", (D. M. Bibby, C. D. Chang, R. Howe, F., and S. Yurchak, eds.), Elsevier Sci. Pub., The Netherlands, pp 517-521.

IX.C-19. Kikuchi, E., and H. Itoh, 1991. *J. Japan Petrol. Inst.*, **34**, 407.

IX.C-20. Kimoto, K., Y. Kamiya, M. Nonoyama and R. Uyeda, 1963. *Japan J. Appl. Phys.*, **2**, 702.

IX.C-21. Kölbel, H., and M. Ralek, 1980. *Catal. Rev.-Sci. Eng.*, **21**, 225.

IX.C-22. Schliebs, B., and J. Gaube, 1985. *Ber. Bunsenges. Phys. Chem.*, **89**, 68.

IX.C-23. Storch, H. H., N. Golumbic and R. B. Anderson, 1951. "The Fischer-Tropsch and Related Synthesis", Wiley, New York.

IX.C-24. Tau, L.-M., H. A. Dabbagh and B. H. Davis, 1990. *Energy & Fuels*, **4**, 94.

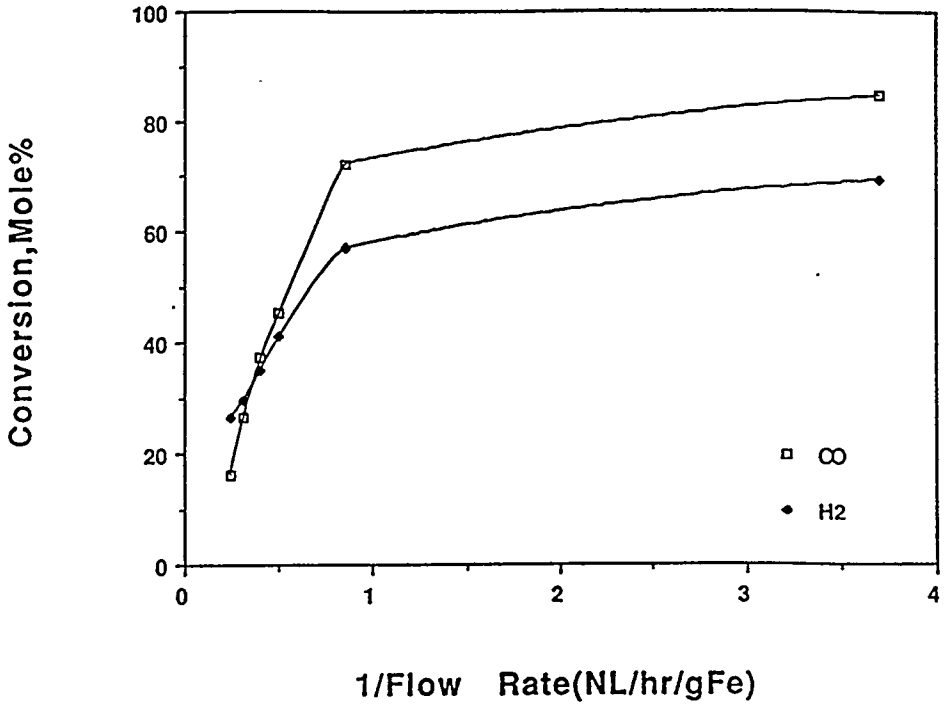

Figure IX.C-1. Conversion of CO (○) and H_2 (◆) versus the reciprocal space velocity (slurry, 20 wt.%; temp., 260°C; total pressure, 8 atm abs.; H_2/CO = 1:1).

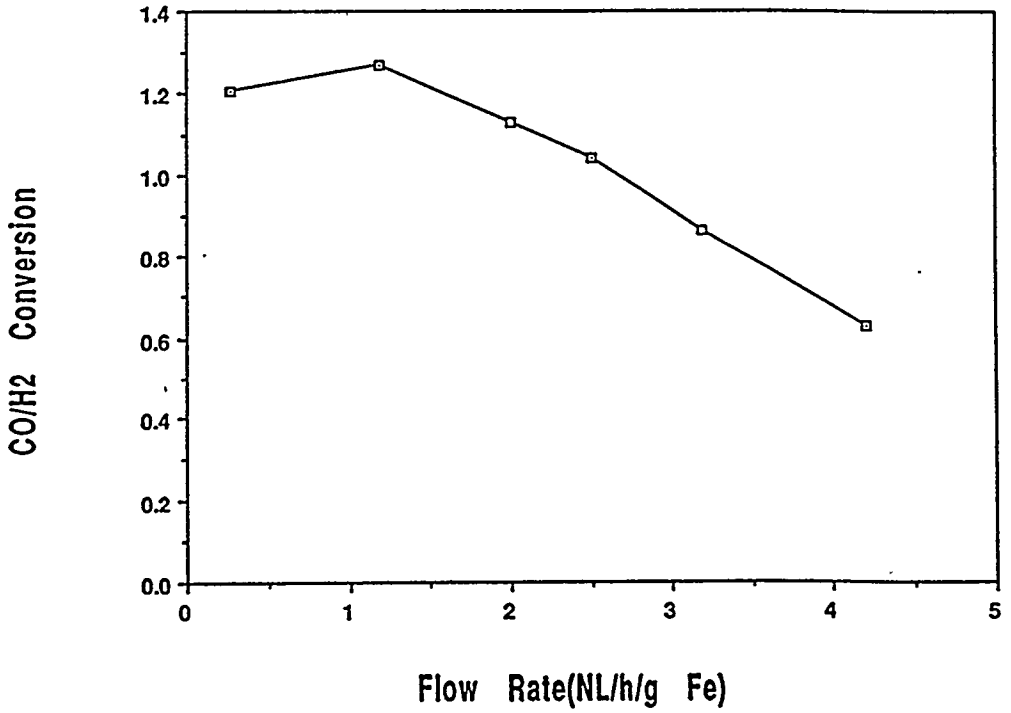

Figure IX.C-2. Variation of the ratio of CO to H_2 conversion versus total flow rate (slurry, 20 wt.%; temp., 260°C; total pressure, 8 atm abs.; H_2/CO = 1:1).

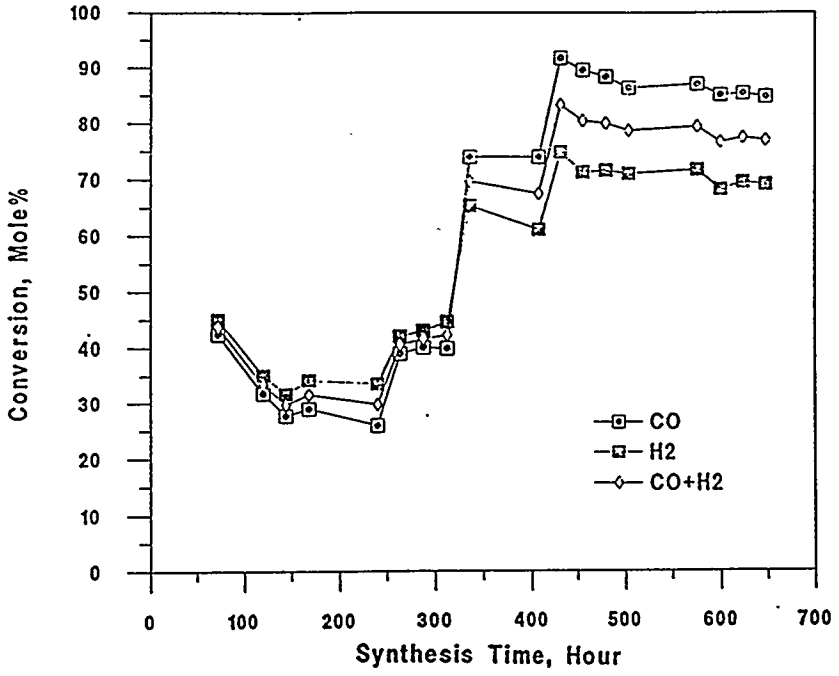

Figure IX.C-3. Conversion of CO (○), H_2 (■) and (CO + H_2) (○) during the initial exposure of catalyst to syngas (slurry, 20 wt.%; temp., 260°C; total pressure, 8 atm abs.; H_2/CO = 1:1; flow rate, 0.27 NL/hr/g Fe).

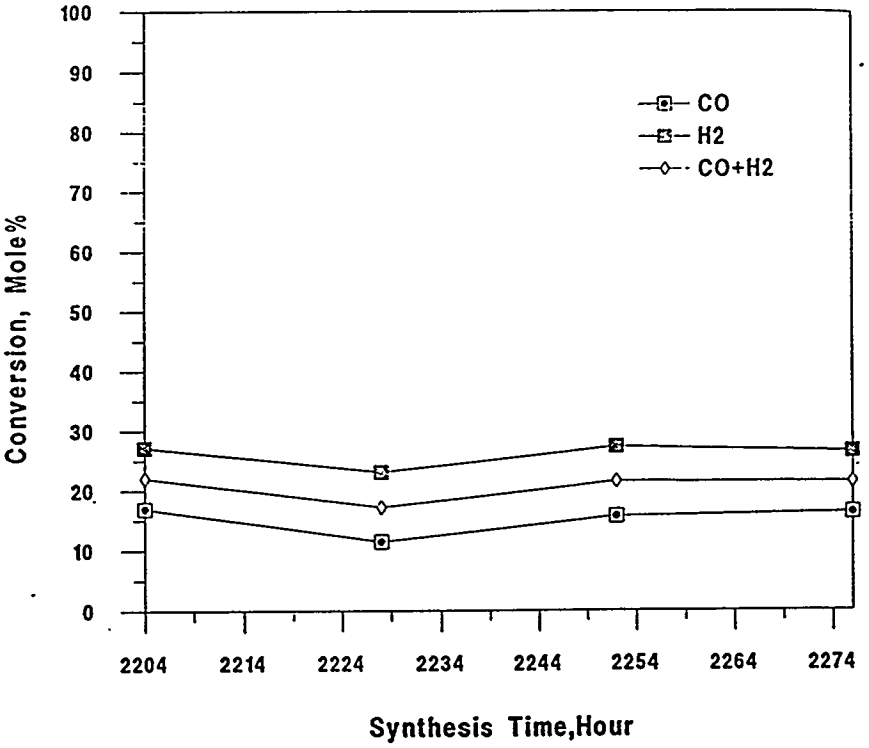

Figure IX.C-4. Conversion of CO (○), H_2 (■) and (CO + H_2) (○) during the initial exposure of catalyst to syngas (slurry, 20 wt.%; temp., 260°C; total pressure, 8 atm abs.; H_2/CO = 1:1; flow rate, 4.2 NL/hr/g Fe).

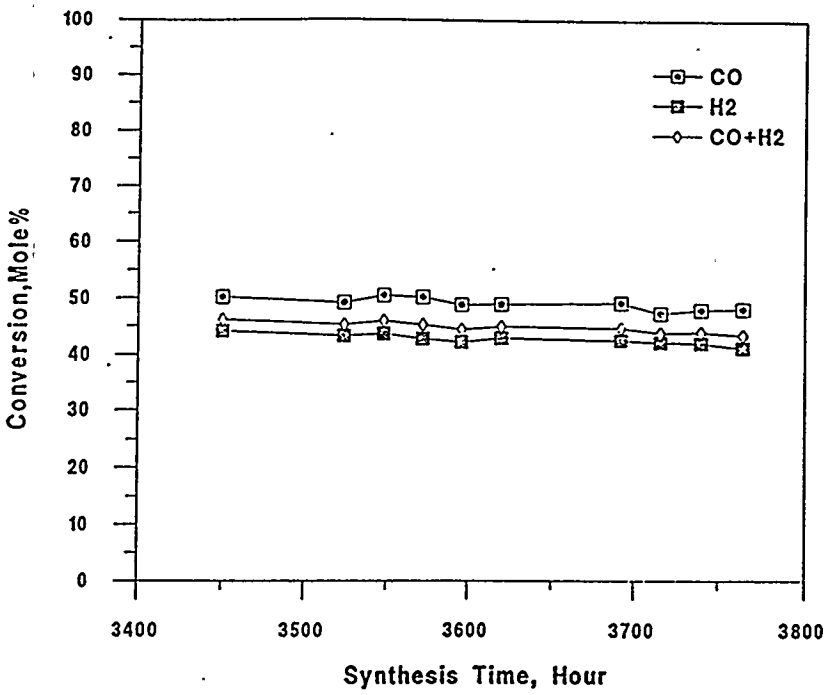

Figure IX.C-5. Conversion of CO (○), H_2 (■) and (CO + H_2) (○) during the initial exposure of catalyst to syngas (slurry, 20 wt.%; temp., 260°C; total pressure, 8 atm abs.; H_2/CO = 2:0; flow rate, 2.5 NL/hr/g Fe).

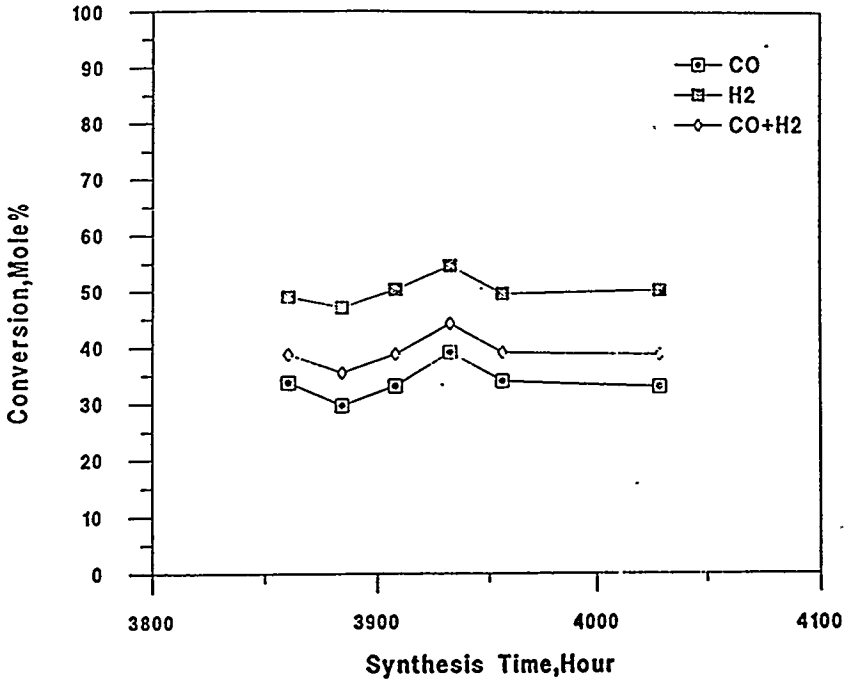

Figure IX.C-6. Conversion of CO (○), H_2 (■) and (CO + H_2) (○) during the initial exposure of catalyst to syngas (slurry, 20 wt.%; temp., 260°C; total pressure, 8 atm abs.; H_2/CO = 0:5; flow rate, 2.5 NL/hr/g Fe).

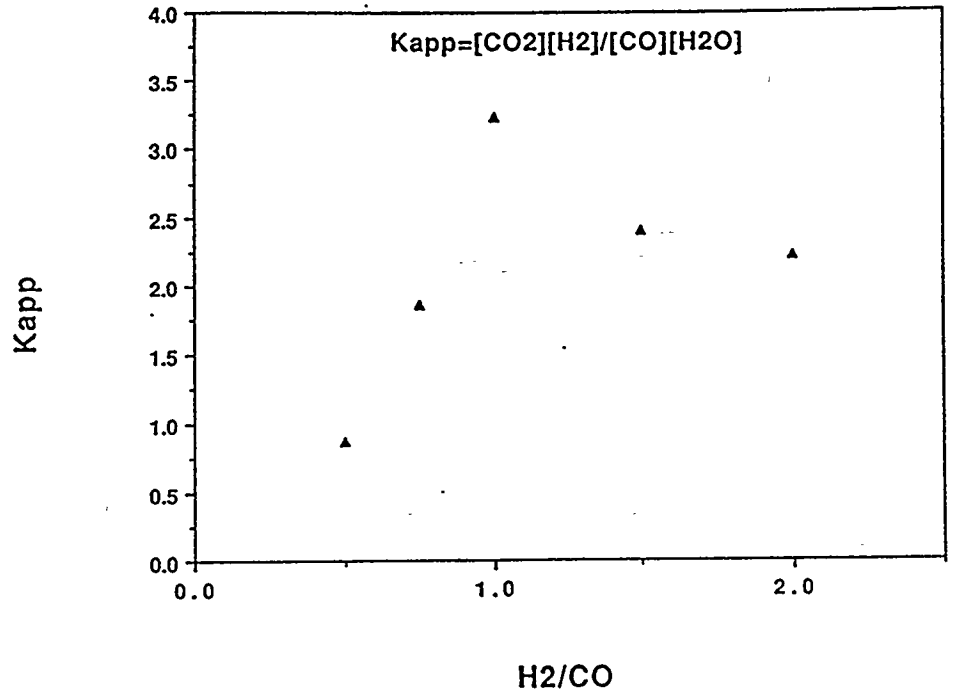

Figure IX.C-7. The apparent water-gas-shift constant (K_{app}) versus H_2/CO ratio of the syngas (slurry, 20 wt.%; temp., 260°C; total pressure, 8 atm abs.; flow rate, 2.5 NL/hr/g Fe).

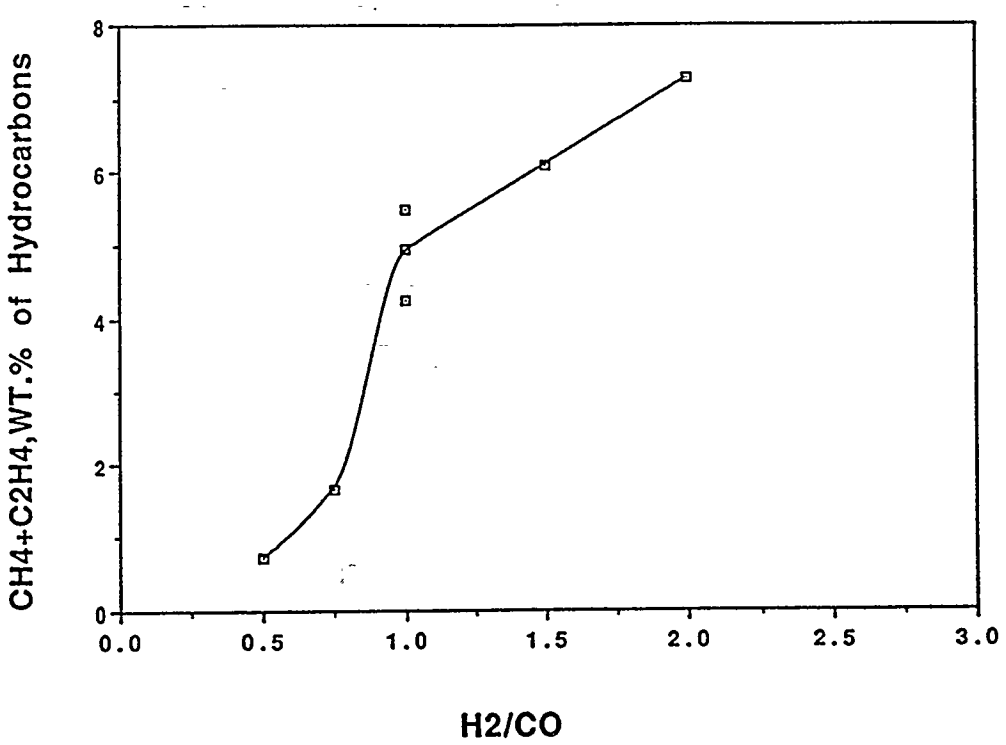

Figure IX.C-8. Dependence of methane plus ethane wt.% of total hydrocarbons with varying H_2/CO ratios.

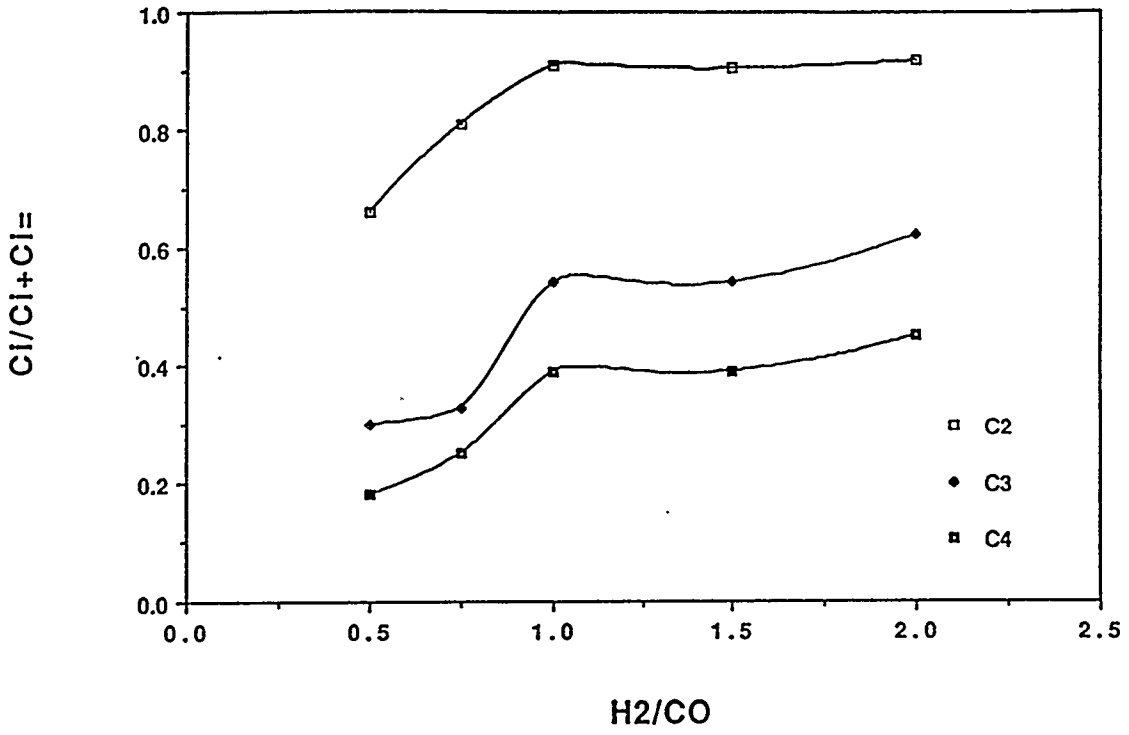

Figure IX.C-9. Variation of the alkane fraction for the C_2 - C_4 products versus H_2/CO ratios.

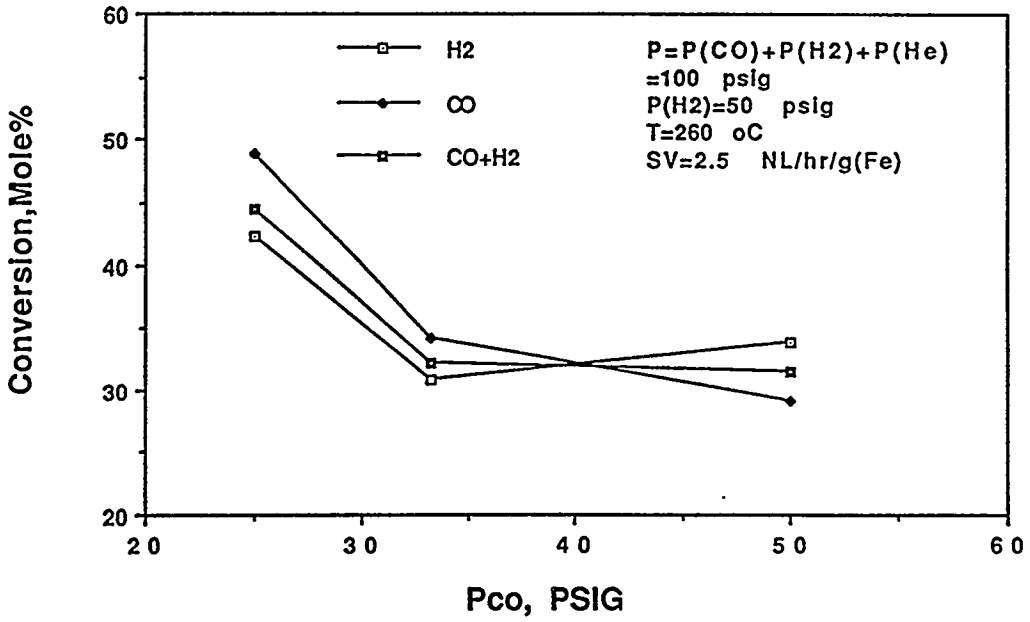

Figure IX.C-10. Conversion (H_2 (○), CO (◆) and (CO + H_2) (■)) versus the partial pressure of CO in the synthesis gas.

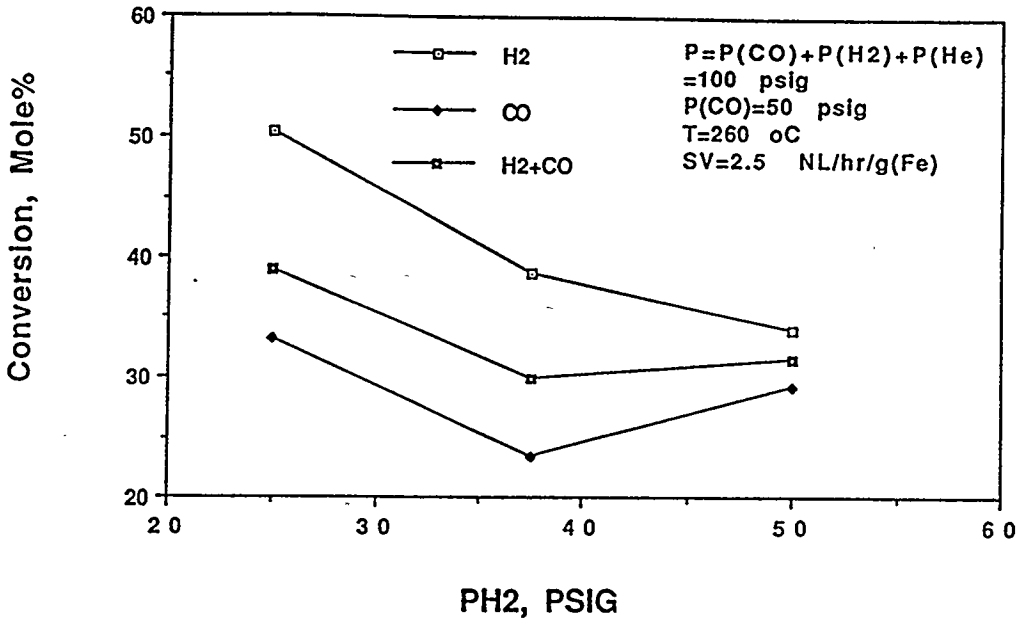

Figure IX.C-11. Conversion (H_2 (○), CO (◆) and (CO + H_2) (■)) versus the partial pressure of H_2 in the synthesis gas.

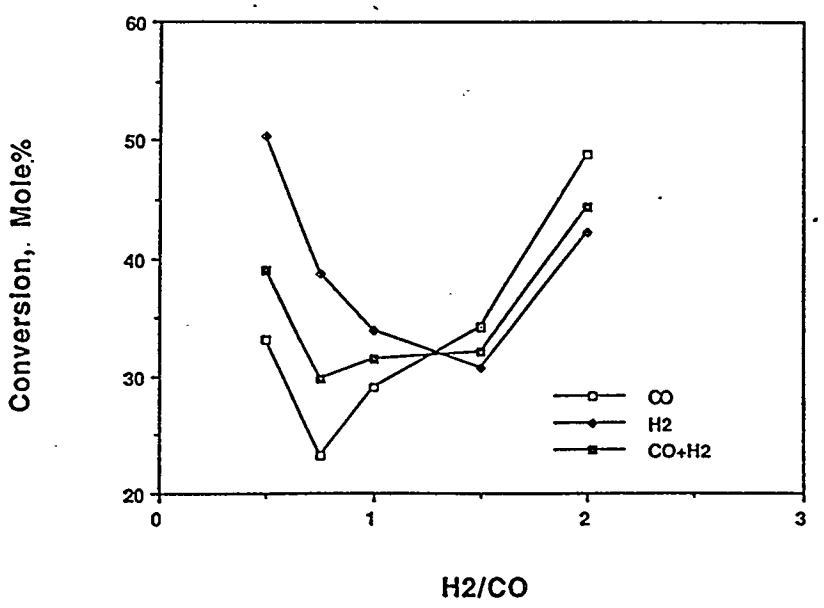

Figure IX.C-12. Conversion (H_2 (○), CO (◆) and (CO + H_2) (■)) versus H_2/CO conversion ratio.

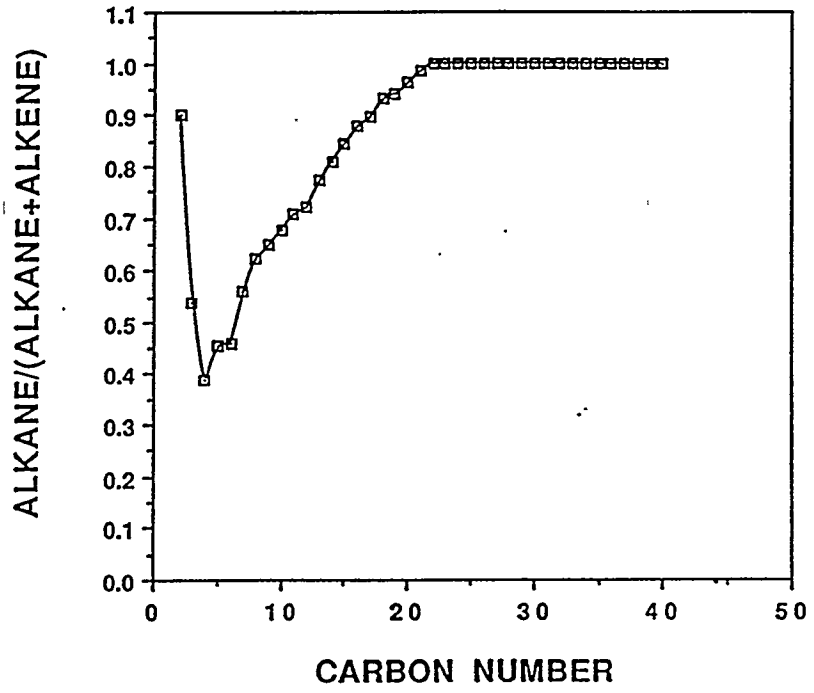

Figure IX.C-13. Alkane fraction for each carbon number versus the carbon number for the ultrafine iron catalyst.

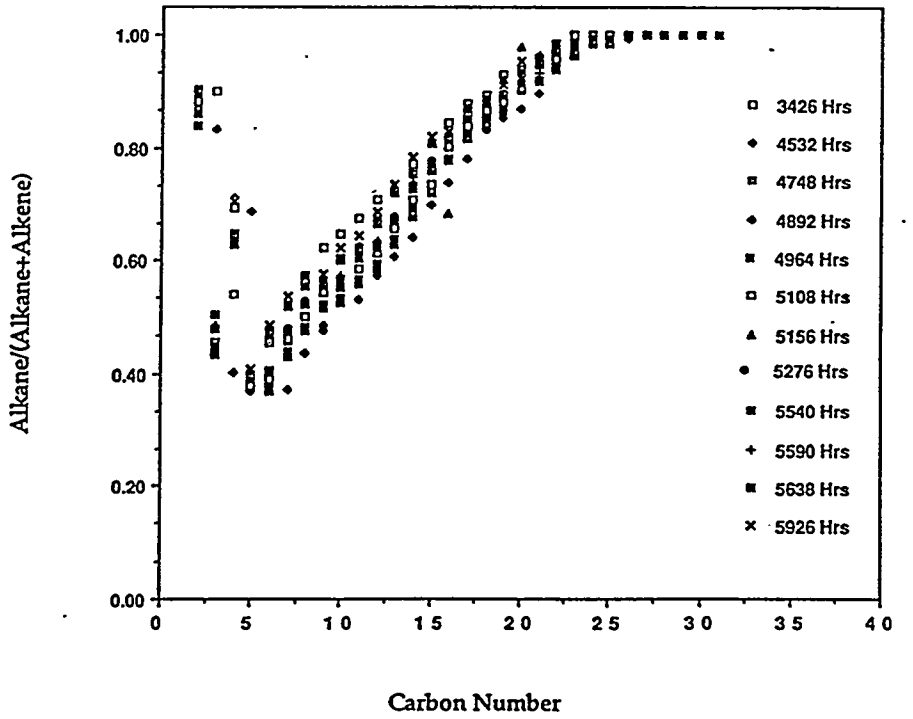

Figure IX.C-14. Alkane fraction for each carbon number versus the carbon number for various times on-stream.

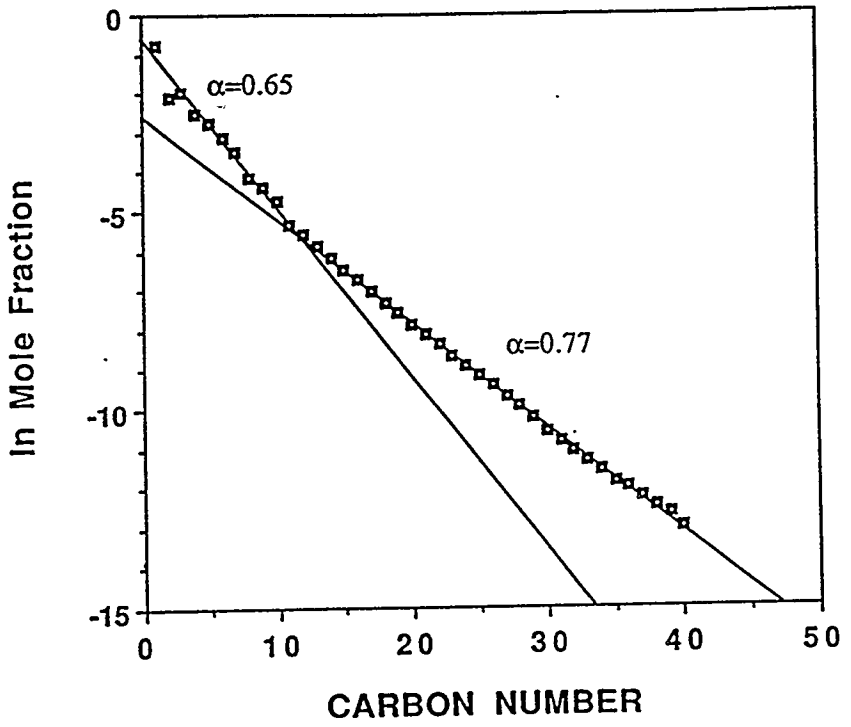

Figure IX.C-15. Anderson-Schulz-Flory (ASF) plot for the products from the unpromoted ultrafine iron oxide catalyst.

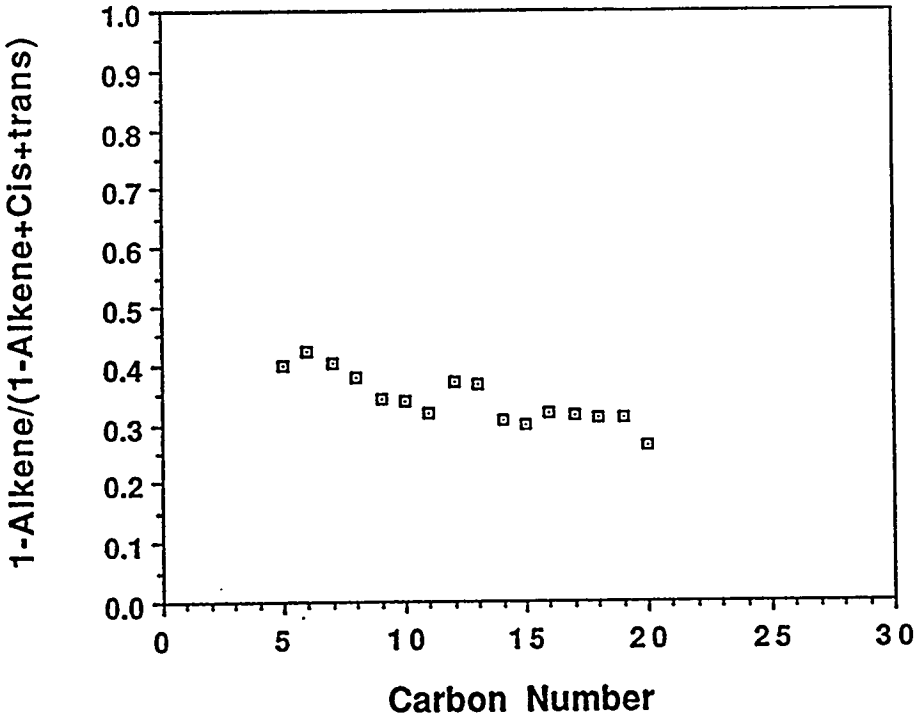

Figure IX.C-16. Fraction of alpha-olefin ($\alpha/(\alpha + \beta)$) versus carbon number for the products from the unpromoted ultrafine iron oxide catalyst.

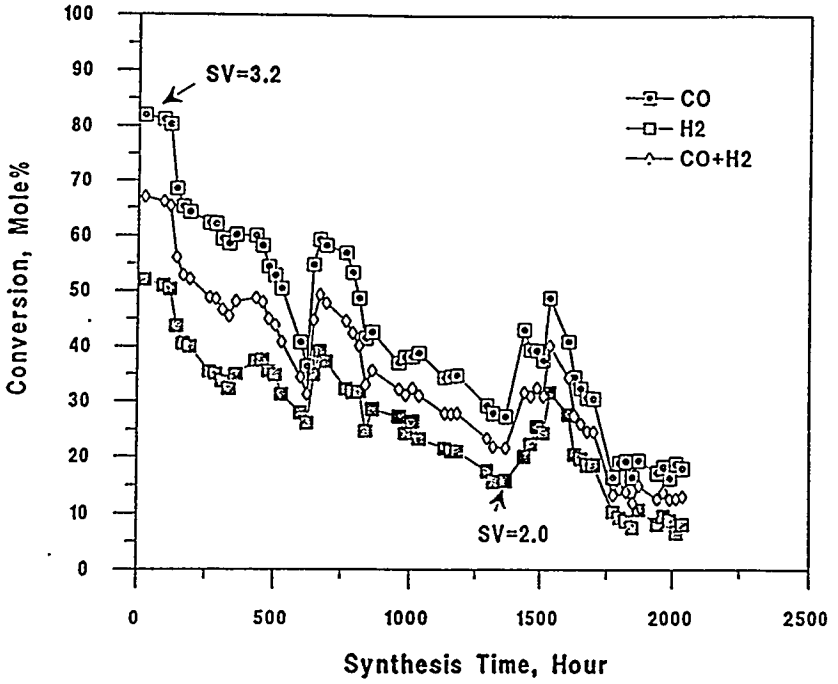

Figure IX.C-17. Conversion ((○), CO; (◆), H_2; (■), (CO + H_2)) versus time of exposure to synthesis gas for the ultrafine iron oxide catalyst containing 0.5 wt.% K (260°C, 8 atm. absolute, H_2/CO = 1, flow rate = 3.2 NL/hr/g Fe, 2.0 NL/hr/g Fe after 1368 hours).

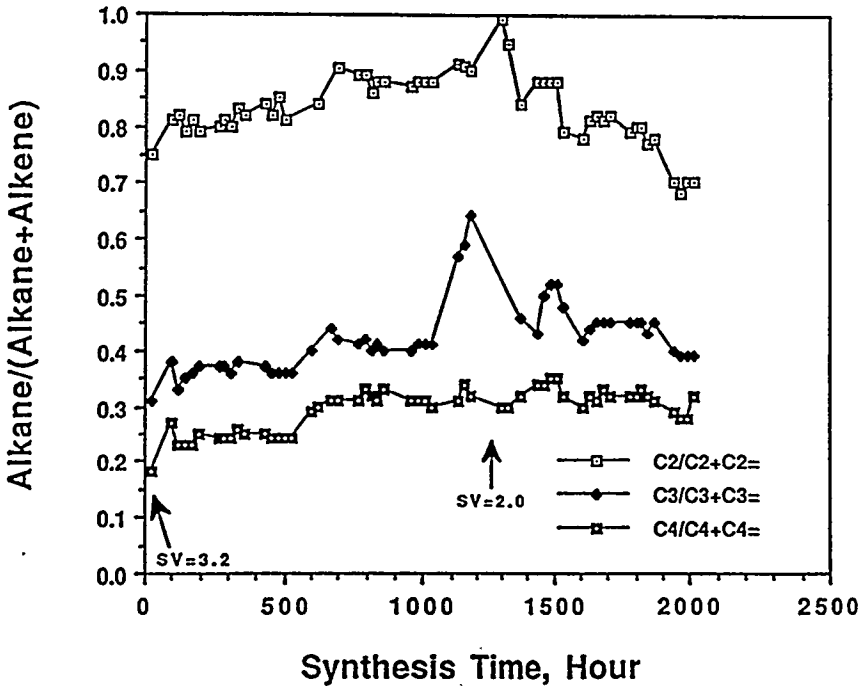

Figure IX.C-18. Alkane fraction for C_2 - C_4 products with increasing synthesis time for the K promoted ultrafine iron catalyst.

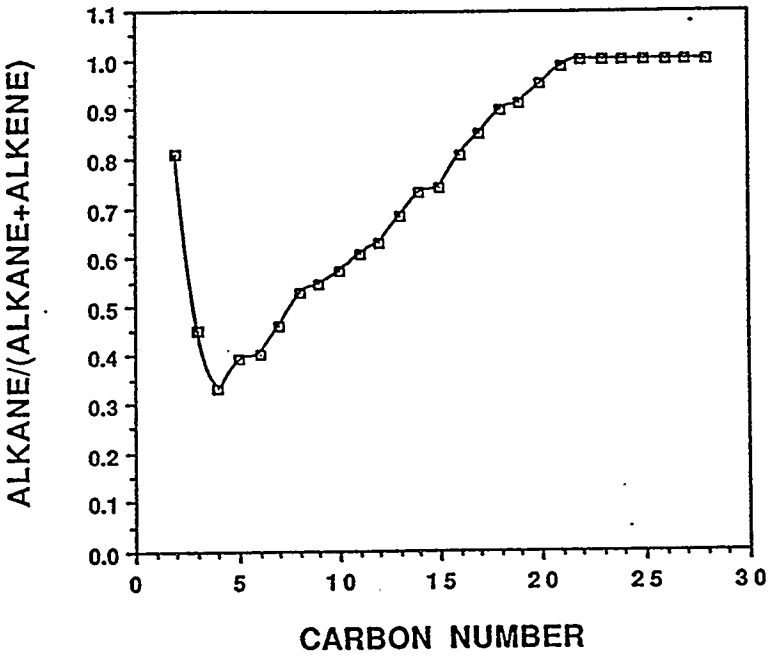

Figure IX.C-19. Alkane fraction for each carbon number versus the carbon number for the K promoted ultrafine iron catalyst.

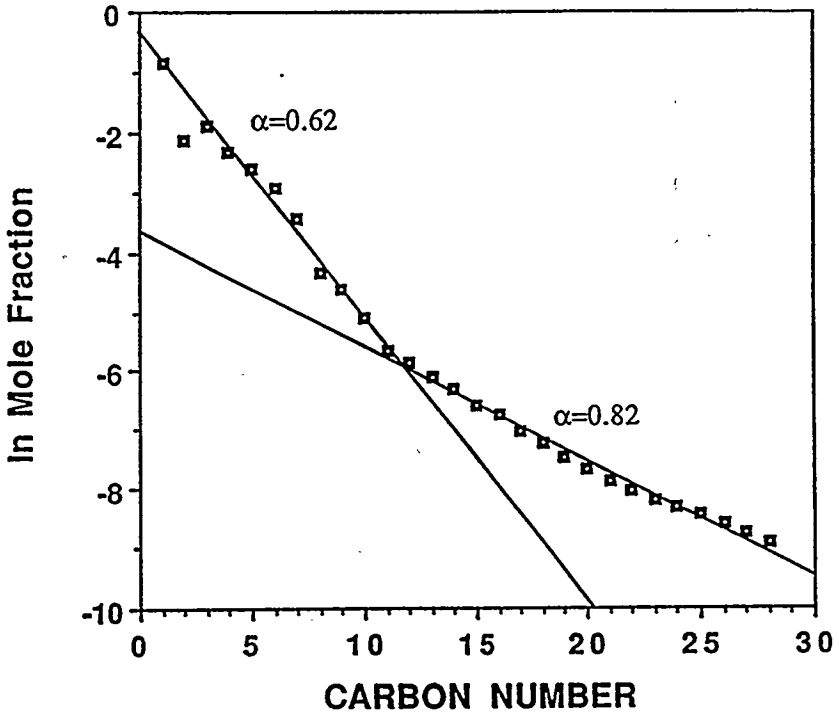

Figure IX.C-20. Anderson-Schulz-Flory (ASF) plot for the products from the K promoted ultrafine iron oxide catalyst.